

Article

Mathematical Modeling of Pseudoplastic Nanofluid Natural Convection in a Cavity with a Heat-Generating Unit and Solid Finned Heat Sink

Daria S. Loenko and Mikhail A. Sheremet *

Laboratory on Convective Heat and Mass Transfer, Tomsk State University, 634050 Tomsk, Russia;
d.s.loenko@mail.tsu.ru

* Correspondence: sheremet@math.tsu.ru; Tel.: +7-3822-529740

Abstract: The power-law nanofluid natural convection in a chamber with a thermally generating unit and a solid ribbed structure has been studied in this work. A mixture of carboxymethylcellulose with water and copper nanoparticles is a working fluid illustrating pseudoplastic properties. The effective properties of the nanofluid have been described by experimental correlations reflecting the temperature effect. The governing equations have been formulated on the basis of the conservation laws of mass, momentum and energy employing non-primitive parameters such as stream function and vorticity. The defined boundary value problem has been worked out by the finite difference technique using an independently developed calculation system. The Rayleigh number is fixed for analysis ($Ra = 10^5$). The paper analyzes the influence of the nanoparticles volume fraction, an increase in which reduces the temperature in the case of the one edge presence. An analysis of the rib height has shown that its growth leads to a weakening of the convective heat transfer, but at the same time, the source temperature also decreases. Increasing the number of fins from 1 to 3 also helps to reduce the average temperature of the heat-generated element by 15%.



Citation: Loenko, D.S.; Sheremet, M.A. Mathematical Modeling of Pseudoplastic Nanofluid Natural Convection in a Cavity with a Heat-Generating Unit and Solid Finned Heat Sink. *Mathematics* **2023**, *11*, 3868. <https://doi.org/10.3390/math11183868>

Academic Editor: Ramoshweu Solomon Lebelo

Received: 3 August 2023

Revised: 4 September 2023

Accepted: 8 September 2023

Published: 11 September 2023



Copyright: © 2023 by the authors. Licensee MDPI, Basel, Switzerland. This article is an open access article distributed under the terms and conditions of the Creative Commons Attribution (CC BY) license (<https://creativecommons.org/licenses/by/4.0/>).

Keywords: natural convection; pseudoplastic nanofluid; square enclosure; mathematical modeling; finned structure; radiator

MSC: 76A05; 76M20; 76R10; 80A20

1. Introduction

Cooling or heating due to convective heat transfer is one of the most attractive mechanisms of heat transfer in thermal engineering systems, as it has a number of advantages in simplicity and economy. Natural convection in various geometric configurations has a wide range of applications in many fields of technology, such as aerospace engineering, textile engineering, the automotive industry, heat storage systems, microelectronic devices design, etc. But researchers are constantly looking for more efficient heat transfer modes that can be obtained by changing the geometry of the system or working fluid [1–3]. One way to improve the heat transfer is to use expanded surfaces or fins. In many supplements in mechanical engineering, chemical engineering, power engineering, heat recovery, surface research, etc., fins have a wide range of applications. Based on this, many researchers investigate the efficiency of their use through analytical, numerical, or experimental studies [4]. Another way to intensify the heat transfer is to use highly thermally conductive liquids as working media. These media include nanofluids, which consist of a base medium and highly thermally conductive solid additives, which increase the thermal characteristics of the entire liquid.

The combination of these mentioned improvements can lead to more efficient cooling/heating of various elements. For example, Hidki et al. [5] have studied the thermal

convection of a $\text{Cu}+\text{Al}_2\text{O}_3$ /water hybrid nanofluid in a closed chamber with two heat-generating blocks. Simulations have shown that the presence of solid particles reduces the temperature of the blocks by up to 18%. Mounting the fins on the blocks surface reduces their temperature by up to 12%. The influence of the heated fin presence on the hybrid nanofluid natural convection has been studied by Iftikhar et al. [6]. The working medium is a mixture of ethylene glycol with copper and silver nanoparticles. The outcomes have demonstrated that the presence of nanoadditives enhances the fluid flow rate by 47.4%, in contrast to the case of a pure base medium. The work of M. Hatami [4] is similar to the study of Iftikhar et al. [6], but the side walls and the upper one are cooled. Additionally, two types of nanoparticles, namely, TiO_2 and Al_2O_3 , are studied. The authors have found that the use of titanium oxide nanoparticles leads to an intensification of the convective energy transport in the chamber. The influence of the ribs number, nanoparticles volume fraction and Rayleigh number on the thermal convective energy transport of the $\text{Cu}/\text{H}_2\text{O}$ nanofluid in the annular space has been investigated by Waqas et al. [7]. The analysis has demonstrated that a growth in the solid particles concentration and Rayleigh number improves the energy transport and flow velocity. Shahsavari et al. [8] have studied the Ag/water nanofluid natural convection in a concentric channel. Additionally, entropy generation has been analyzed. The authors have found that a growth in the number of edges results in a rise in the mean Nusselt number to 35.50% and entropy production rate to 39.07%. A similar geometry was used by Tayebi et al. in [9] where the authors also investigated the influence of the Lorentz force on the $\text{Al}_2\text{O}_3/\text{H}_2\text{O}$ nanofluid thermogravitational convection. It has been shown that the strength of the convective energy transport decreases with a growth of the fins size and the Hartmann number, but increases with Ra and ϕ . Yasmin et al. [10] used a hexagonal nanofluid chamber under the impact of a ribbed circular cylinder. The horizontal borders of the cavity are hot, the rest are cold. As a result of the study, it has been ascertained that a growth in the fins' height and the nanoadditives' concentration improves the energy transport. Hejri and Malekshah [11] have analyzed the best geometric characteristics for a cooling system consisting of a finned structure filled with $\text{CuO}/\text{H}_2\text{O}$ nanofluid. The authors have also studied the influence of the shape of nanoparticles on the process. The analysis has shown that thin ribs and plate-shaped particles are more efficient for the considered phenomenon. The presence of two heat-conducting ribs in a tilted porous chamber filled with ferrofluid $\text{Fe}_3\text{O}_4/\text{H}_2\text{O}$ has been studied by Al-Farhany et al. [12]. The authors found that the fins' length and the distance between them have a significant effect on the intensity of the convective heat transfer. We should note that the addition of Fe_3O_4 nanoparticles intensifies the convective heat transfer regardless of the ribs' length and the distance between them. A similar geometry was investigated by Yan et al. [13], where the main difference is that the edges can have different inclination angles. The influence of the Al_2O_3 nanoparticles' shape has been also studied in this work. The main conclusion is that an increase in the concentration of nanoparticles does not always lead to an intensification of the convective heat transfer. The highest energy transport coefficient was obtained in the case of inclined fins. An analogous system has been studied by Siavashi et al. [14] but with porous fins. The authors revealed that a growth in Da enhances the heat transfer in the cavity. An increase in the number of ribs or their length does not have an essential impact on the mean Nusselt number.

Esfe et al. [15] modeled a 3D free convection in a differentially heated chamber under the porous ribs; influence on a hot wall. $\text{CuO}/\text{H}_2\text{O}$ nanofluid has been used as a working medium. The simulation results have demonstrated that an addition of porous fins decreases the fluid flow rate, and a growth in the nanoadditives' volume fraction leads to an intensification of convective energy transport. Gireesha et al. [16] considered the free-convective energy transport between a hybrid $\text{Ag}+\text{MgO}/\text{H}_2\text{O}$ nanofluid and a hot moving porous fin. It has been found that the presence of nanoadditives intensifies the energy transport, and an increase in the Biot number increases the rate of the heat removal from the fin surface. A ribbed square body with a rotating hot rectangular block inside has been examined by Aly et al. [17]. The chamber was filled with $\text{Cu}/\text{H}_2\text{O}$ nanofluid,

and the hot block also had two hot ribs on the sides. The results demonstrated that the presence of ribs reduces the distribution of isotherms and lines of constant concentration inside the cavity and changing the block angle from 0° to 90° can increase the flow rate by 9.59% and 31.53%, respectively. Ganesh et al. [1] performed the mathematical modeling of the Casson nanofluid MWCNT/sodium alginate flow in a casing with wavy horizontal walls. In the housing center, there is a circular heat-insulated barrier and two differentially heated fins. The simulation has shown that a growth in the Rayleigh number, Casson parameter, nanoadditives concentration, and wall waviness amplitude increases the heat transfer rate. The work of Siva et al. [18] is devoted to an analytical study of the electromagnetic hydrodynamic flow of a non-Newtonian fluid in a microchannel. The authors found that an increase in couple stresses leads to an increase in the flow velocity, but the critical Hartmann number is unchanged. Mehta and Mondal [19] carried out a numerical simulation of a natural convective heat transfer in a cavity with wavy walls, which was filled with MWCNT+Fe₃O₄/water nanofluid. The performed analysis showed that an increase in the volume fraction of nanoparticles and the amplitude of the wall wave leads to an increase in the values of the average Nusselt number. Mondal and Wongwises [20] studied the unsteady electro-MHD nanofluid flow in a rotating channel. The authors showed that the combination of the Coriolis and Lorentz forces with the rheological liquid nature has an interesting result for the flow reversal in the channel. Moreover, for a higher-rotation Reynolds number, the flow reversal owing to the strong Coriolis force influence is impossible due to a growth in the nanofluid's effective viscosity.

A brief analysis of studies of the convective heat transfer of nanofluids in various cavities with ribs showed that this topic is very popular and useful from a theoretical and practical point of view. However, there are still many unexplored phenomena in this area. Therefore, the purpose of this work is to evaluate the efficiency of using a ribbed solid structure for cooling a local heat source employing laminar free-convective energy transfer of a power law nanofluid. The novelty of this study is an analysis of the combined effect of the pseudoplastic nanofluid and solid finned heat sink on the cooling of the heat-generating element. Moreover, the nanofluid's physical properties have been described using experimentally based correlations with the temperature influence. At the same time, the computational analysis was conducted using non-primitive variables that allow reducing the computational time and improving the physical analysis. Obtained results can be used in the modeling and optimizing of the passive cooling systems for various electronic systems.

2. Formulation of the Problem

The geometric scheme of the solution region (see Figure 1) is a square closed cavity, the upper and part of the side borders of which are maintained at a fixed low temperature T_c . A heating element of the fixed volumetric thermal production Q is placed in the center of the chamber lower wall. Above the source there is a heat-conducting copper profile, along the perimeter of which the outer walls are heat-insulated. The height of the ribs H varies during the study. The cavity is filled with a suspension of carboxymethylcellulose (CMC) with water and copper nanoparticles. The thermal characteristics of the materials used are presented in Table 1. The analyzed finned heat sink with nanoenhanced CMC/water suspension can be considered as a passive cooling system for more effective thermal energy removal from the heat-generating element. Such a combination of two different approaches allows enhancing the heat removal compared to each of these techniques.

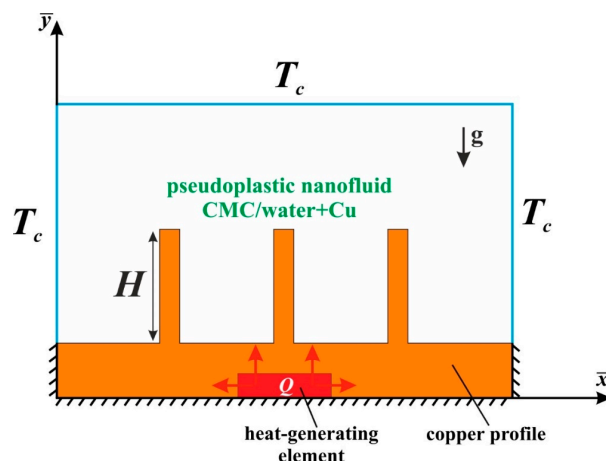


Figure 1. Geometry for the considered problem.

Table 1. Thermal properties of materials [21,22].

Properties	c_p [J/kg·K]	ρ [kg/m ³]	k [W/m·K]
Base fluid			
CMC (0.1%)/water	4179	997.1	0.613
Nanoparticles (Cu)	385	8933	400
Heat source (silicon)	710	2330	150
Ribbed heat sink (Cu)	385	8920	400

The pseudoplastic behavior of the liquid motion is defined by the Ostwald–deWaele power law [23]:

$$\tau_{ij} = 2\mu_{nf}D_{ij} \tag{1}$$

The effective viscosity coefficient of a nanofluid is simulated employing the relation of Guo et al. [24]:

$$\frac{\mu_{nf}}{\mu_{bf}} = \left(1 + 2.5\phi + 6.5\phi^2\right) \left(1 + 350\frac{\phi}{d_p}\right) \tag{2}$$

The viscosity of the host liquid was defined using the relationship: $\mu_{bf} = K(2D_{kl}D_{kl})^{\frac{n-2}{2}}$. Here, K is the flux density factor; D_{kl} are components of the strain rate tensor; n is the fluid behavior index, which is equal to 0.91. Considering that for $n < 1$, the working fluid has a pseudoplastic nature. Such fluids are described by viscosity that reduces with a growth in the strain rate, which is very efficient for the cooling problems.

The nanoliquid heat conductivity was calculated using the experimental correlation of Jang and Choi [25]:

$$\frac{k_{nf}}{k_{bf}} = (1 - \phi) + 0.01\frac{k_p}{k_{bf}}\phi + \left(18 \cdot 10^6\right)\frac{d_{bf}}{d_p}Re^2Pr\phi \tag{3}$$

The control equations reflecting the process of laminar transient convective energy transport employing the Oberbeck–Boussinesq approach based on the dimensional primitive variables “velocity and pressure” are:

$$\frac{\partial \bar{u}}{\partial \bar{x}} + \frac{\partial \bar{v}}{\partial \bar{y}} = 0 \tag{4}$$

$$\rho_{nf} \left(\frac{\partial \bar{u}}{\partial t} + \bar{u} \frac{\partial \bar{u}}{\partial \bar{x}} + \bar{v} \frac{\partial \bar{u}}{\partial \bar{y}} \right) = -\frac{\partial \bar{p}}{\partial \bar{x}} + 2\frac{\partial}{\partial \bar{x}} \left[\mu_{nf} \frac{\partial \bar{u}}{\partial \bar{x}} \right] + \frac{\partial}{\partial \bar{y}} \left[\mu_{nf} \left(\frac{\partial \bar{u}}{\partial \bar{y}} + \frac{\partial \bar{v}}{\partial \bar{x}} \right) \right] \tag{5}$$

$$\rho_{nf} \left(\frac{\partial \bar{v}}{\partial t} + \bar{u} \frac{\partial \bar{v}}{\partial \bar{x}} + \bar{v} \frac{\partial \bar{v}}{\partial \bar{y}} \right) = -\frac{\partial \bar{p}}{\partial \bar{y}} + \frac{\partial}{\partial \bar{x}} \left[\mu_{nf} \left(\frac{\partial \bar{u}}{\partial \bar{y}} + \frac{\partial \bar{v}}{\partial \bar{x}} \right) \right] + 2 \frac{\partial}{\partial \bar{y}} \left[\mu_{nf} \frac{\partial \bar{v}}{\partial \bar{y}} \right] + g(\rho\beta)_{nf}(T - T_c) \quad (6)$$

$$(\rho c)_{nf} \left(\frac{\partial T}{\partial t} + \bar{u} \frac{\partial T}{\partial \bar{x}} + \bar{v} \frac{\partial T}{\partial \bar{y}} \right) = \frac{\partial}{\partial \bar{x}} \left(k_{nf} \frac{\partial T}{\partial \bar{x}} \right) + \frac{\partial}{\partial \bar{y}} \left(k_{nf} \frac{\partial T}{\partial \bar{y}} \right) \quad (7)$$

Heat conduction equations for the energy source and the solid finned heat sink are:

$$(\rho c)_{hs} \frac{\partial T}{\partial t} = k_{hs} \left(\frac{\partial^2 T}{\partial \bar{x}^2} + \frac{\partial^2 T}{\partial \bar{y}^2} \right) + Q \quad (8)$$

$$(\rho c)_r \frac{\partial T}{\partial t} = k_r \left(\frac{\partial^2 T}{\partial \bar{x}^2} + \frac{\partial^2 T}{\partial \bar{y}^2} \right) \quad (9)$$

To reduce the mathematical difficulties, the stream function $\bar{\Psi}$ ($\bar{u} = \partial \bar{\Psi} / \partial \bar{y}$, $\bar{v} = -\partial \bar{\Psi} / \partial \bar{x}$) and vorticity ($\bar{\omega} = \partial \bar{v} / \partial \bar{x} - \partial \bar{u} / \partial \bar{y}$), as well as reference parameters presented in Table 2, are introduced into system (4)–(9). L is chosen as the length scale and $\Delta T = QL^2/k_{hs}$ is used for the temperature difference.

Table 2. Reference parameters.

Parameters	Formula
Velocity	$\sqrt{g\beta L \Delta T}$
Time	$\sqrt{L / (g\beta \Delta T)}$
Stream function	$\sqrt{g\beta L^3 \Delta T}$
Vorticity	$\sqrt{g\beta \Delta T / L}$
Temperature	$\Delta T = QL^2 / k_{hs}$

As a result, the non-dimensional governing equations are:

$$\frac{\partial^2 \Psi}{\partial X^2} + \frac{\partial^2 \Psi}{\partial Y^2} = -\Omega \quad (10)$$

$$\frac{\partial \Omega}{\partial \tau} + \frac{\partial \Psi}{\partial Y} \frac{\partial \Omega}{\partial X} - \frac{\partial \Psi}{\partial X} \frac{\partial \Omega}{\partial Y} = H_1(\phi) \left(\frac{Ra}{Pr} \right)^{\frac{n-2}{2}} \left[\nabla^2(\bar{M}\Omega) + S_\Omega \right] + H_2(\phi) \frac{\partial \Theta}{\partial X} \quad (11)$$

$$\frac{\partial \Theta}{\partial \tau} + \frac{\partial \Psi}{\partial Y} \frac{\partial \Theta}{\partial X} - \frac{\partial \Psi}{\partial X} \frac{\partial \Theta}{\partial Y} = \frac{H_3(\phi)}{\sqrt{Ra \cdot Pr}} \left[\frac{\partial}{\partial X} \left(\frac{k_{nf}}{k_{bf}} \cdot \frac{\partial \Theta}{\partial X} \right) + \frac{\partial}{\partial Y} \left(\frac{k_{nf}}{k_{bf}} \cdot \frac{\partial \Theta}{\partial Y} \right) \right] \quad (12)$$

The heat conduction equations for the energy source and the radiator are:

$$\frac{\partial \Theta_{hs}}{\partial \tau} = \frac{\alpha_{hs} / \alpha_{bf}}{\sqrt{Ra \cdot Pr}} \left(\frac{\partial^2 \Theta_{hs}}{\partial X^2} + \frac{\partial^2 \Theta_{hs}}{\partial Y^2} + 1 \right) \quad (13)$$

$$\frac{\partial \Theta_r}{\partial \tau} = \frac{\alpha_r / \alpha_{bf}}{\sqrt{Ra \cdot Pr}} \left(\frac{\partial^2 \Theta_r}{\partial X^2} + \frac{\partial^2 \Theta_r}{\partial Y^2} \right) \quad (14)$$

Here, the used additional functions are \bar{M} (non-dimensional viscosity of the host liquid), S_Ω (source term) and $H_1(\phi)$, $H_2(\phi)$, $H_3(\phi)$ (additional functions reflecting the thermal characteristics of the nanosuspension). These additional functions can be presented as follows:

$$\bar{M} = \left[4 \left(\frac{\partial^2 \Psi}{\partial X \partial Y} \right)^2 + \left(\frac{\partial^2 \Psi}{\partial Y^2} - \frac{\partial^2 \Psi}{\partial X^2} \right)^2 \right]^{\frac{n-1}{2}}, S_\Omega = 2 \left[\frac{\partial^2 \bar{M}}{\partial X^2} \frac{\partial^2 \Psi}{\partial Y^2} + \frac{\partial^2 \bar{M}}{\partial Y^2} \frac{\partial^2 \Psi}{\partial X^2} - 2 \frac{\partial^2 \bar{M}}{\partial X \partial Y} \frac{\partial^2 \Psi}{\partial X \partial Y} \right]$$

$$H_1(\phi) = \frac{\mu_{nf} \rho_{bf}}{\mu_{bf} \rho_{nf}} = \frac{\mu_{nf} / \mu_{bf}}{(1 - \phi + \phi \rho_p / \rho_{bf})}, H_2(\phi) = \frac{(\rho\beta)_{nf} \rho_{bf}}{(\rho\beta)_{bf} \rho_{nf}} = \frac{1 - \phi + \phi(\rho\beta)_p / (\rho\beta)_{bf}}{1 - \phi + \phi \rho_p / \rho_{bf}},$$

$$H_3(\phi) = \frac{(\rho c)_{bf}}{(\rho c)_{nf}} = \frac{1}{1 - \phi + \phi(\rho c)_p / (\rho c)_{bf}}$$

The initial and boundary conditions for the system (10)–(14) in a dimensionless form are as follows:

$$\begin{aligned} \tau = 0 &\rightarrow \Psi = \Omega = 0, \Theta = 0.0; \\ \tau > 0 &\rightarrow \\ X = 0 \ \& \ X = 1, 0 \leq Y \leq 0.1, \frac{\partial \Theta}{\partial X} = 0; \\ X = 0 \ \& \ X = 1, 0.1 < Y \leq 1, \Psi = 0, \frac{\partial \Psi}{\partial X} = 0, \Theta = 0; \\ Y = 0, 0 &\leq X \leq 1, \frac{\partial \Theta}{\partial Y} = 0; \\ Y = 1, 0 &\leq X \leq 1, \Psi = 0, \frac{\partial \Psi}{\partial Y} = 0, \Theta = 0. \end{aligned}$$

At the heat source surface, one can find: $\Theta_{hs} = \Theta_r, \frac{k_{hs}}{k_r} \frac{\partial \Theta_{hs}}{\partial n} = \frac{\partial \Theta_r}{\partial n}$.

At the radiator surface, we have: $\Psi = 0, \Omega = -\frac{\partial^2 \Psi}{\partial n^2}, \Theta_{nf} = \Theta_{bf}, \frac{k_{nf}}{k_r} \frac{\partial \Theta_{nf}}{\partial n} = \frac{\partial \Theta_r}{\partial n}$.

For a solution to the formulated system of unsteady differential Equations (10)–(14) with the corresponding restrictions, the finite difference technique was used [26–28]. A successive under-relaxation algorithm was used to work out the approximated Poisson equation. The non-dimensional viscosity was discretized employing a regularization technique [26]. The Samarskii locally one-dimensional difference procedure [27,28] was applied to reduce Equations (11) and (12) to the system of one-dimensional equations. Further on, the convective terms were approximated using the donor cells scheme, and the diffusion terms were discretized by central differences. The obtained systems of linear algebraic equations were solved by the Thomas method.

The developed numerical technique and the prepared computation code were verified employing the model problems. Figure 2 demonstrates the geometry of the model problem. Power-law fluid circulates in a differentially heated enclosure. The horizontal walls are thermally insulated. Comparison of the outcomes was performed for the average Nusselt number calculated at the hot wall $\left(Nu_{avg} = -\int_0^1 \frac{\partial \Theta}{\partial X} dY \right)$, depending on time and the fluid behavior index n as shown in Figure 3. Obtained results are represented by white symbols, while the results of [24] are shown in black. It can be seen that the difference in the results does not exceed 4%; this illustrates a very good agreement.

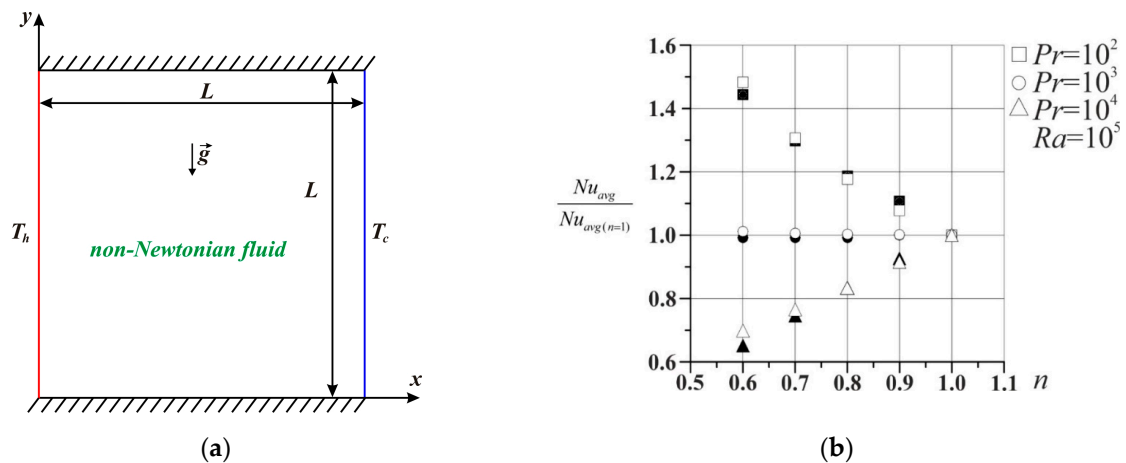


Figure 2. Testing the program code: (a) Model domain of interest; (b) Average Nusselt number behavior in comparison with [29].

An additional study was performed for the mesh effect on the solution convergence using the mean Nusselt number and mean heater temperature presented in Figure 4 for three ribs at $Ra = 10^5$, $\phi = 0.01, \delta = 0.2$. The mean Nusselt number was defined by $Nu_{avg} = -\frac{1}{1.8} \int_0^{1.8} \frac{\partial \Theta}{\partial n} d\zeta$ at the finned heat sink border, where ζ is the natural coordinate along the finned heat sink border. It can be seen that the meshes of 300×300 and 400×400 units did not lead to significant discrepancies; therefore, the further calculations were carried out on a uniform rectangular grid of 300×300 elements to optimize the computation time.

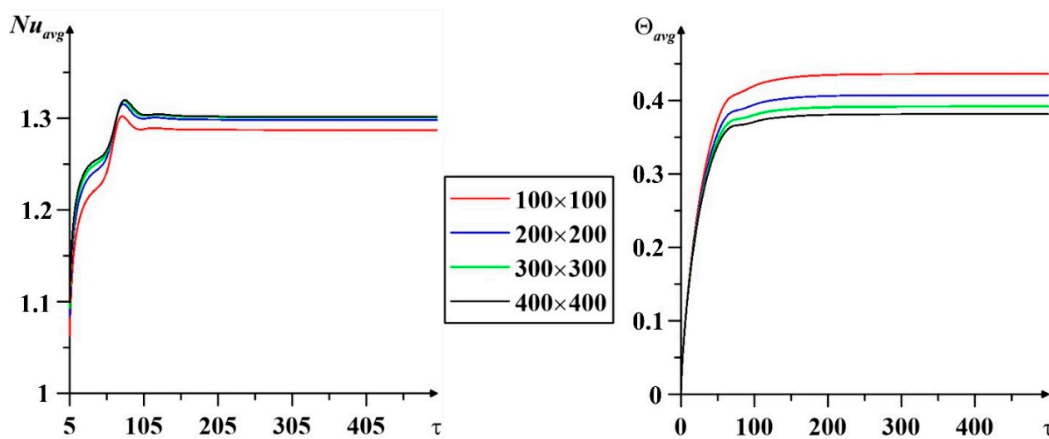


Figure 3. Influence of grid parameters.

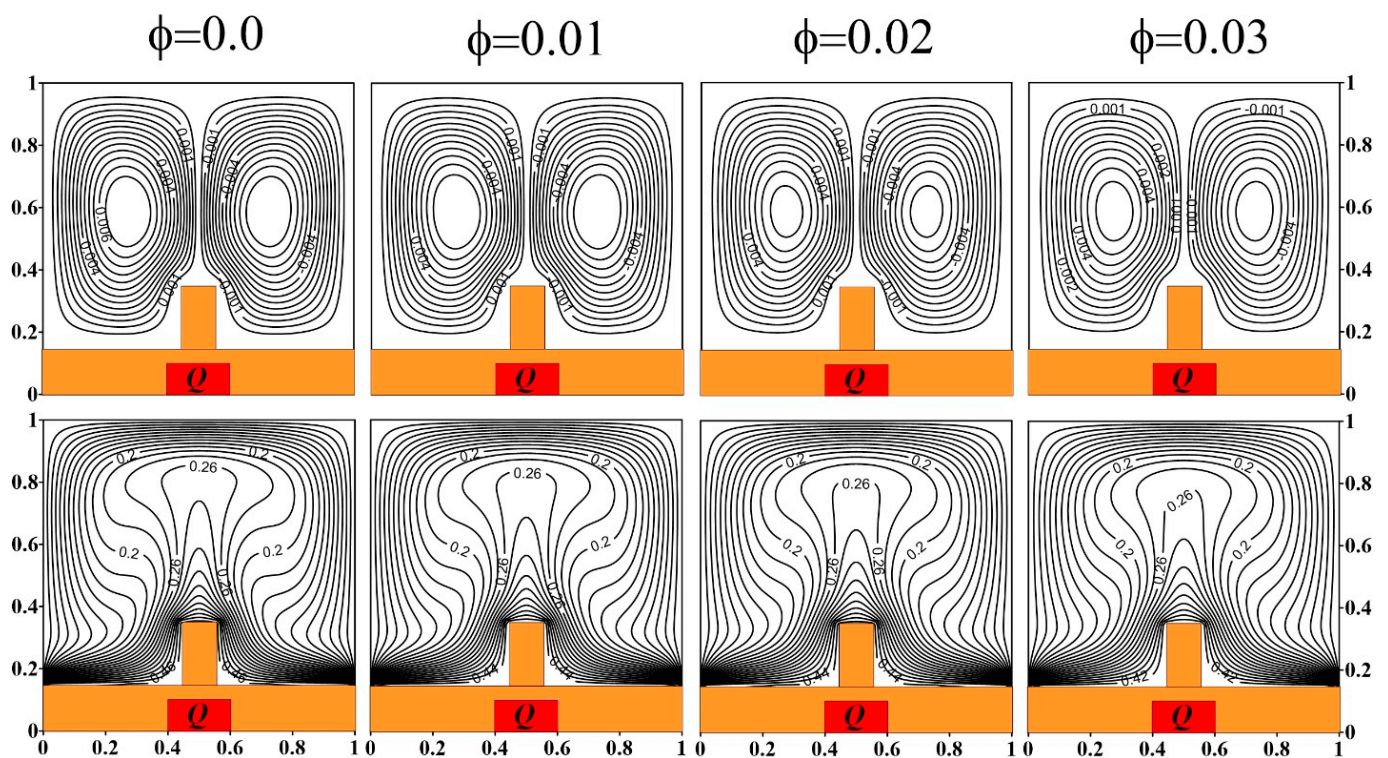


Figure 4. Nanoparticles volume fraction influence on the streamlines and isotherms in the case of one edge at $\delta = 0.2$.

3. Results

This research simulates the process of free convective energy transport of a power-law nanofluid in an enclosure with a heat source and a rib structure. In the course of the study, the impact of the governing characteristics was analyzed, including the volume fraction of nanoparticles ($\phi = 0.0-0.03$), the height of the ribs ($\delta = 0.1-0.3$) and the number of ribs (1–3). The Rayleigh number is fixed for all results ($Ra = 10^5$). The outcomes are shown by the distribution of streamlines and isotherms, as well as curves of the average Nusselt number over the radiator surface and the mean heater temperature.

Figure 4 demonstrates the distribution of streamlines and isotherms depending on the nanoparticles' volume fraction in the case of one heat sink fin at $\delta = 0.2$. The streamlines in the first row illustrate the structure of the nanofluid motion within the chamber. It consists of two symmetrical convective cells, the flow in which occurs in opposite directions. It should be noted that their shape practically does not change with a growth in the nanoadditives' concentration. The second row presents isotherms that reflect the temperature stratification in the chamber. If you look at them

closely, you can see that a two-dimensional heat plume has formed above the rib, which characterizes an intense convective heat transfer. At the same time, according to the isotherm with a value of 0.26, one can trace a slight reduction in the chamber temperature, which indicates the efficiency of using such a cooling system for a heated element.

The impact of the copper nanoparticles' concentration has also been estimated from the values of the mean Nusselt number and mean heater temperature, which are demonstrated in Figure 5 at $\delta = 0.2$. It can be seen that with an increase in ϕ , the average Nusselt number decreases, which indicates a weakening of the convective energy transport in the enclosure. In this case, the average source temperature changes insignificantly, but still decreases with an increase in ϕ . This phenomenon is explained by a growth in the thermal conductivity of the working fluid due to nanoadditives. It should also be noted that the decrease in the values of Nu_{avg} and Θ_{avg} occurs by the same amount with an increase in ϕ . That is, Nu_{avg} decreases by 0.2, and Θ_{avg} by 0.01 with a rise in the nanoadditives' concentration.

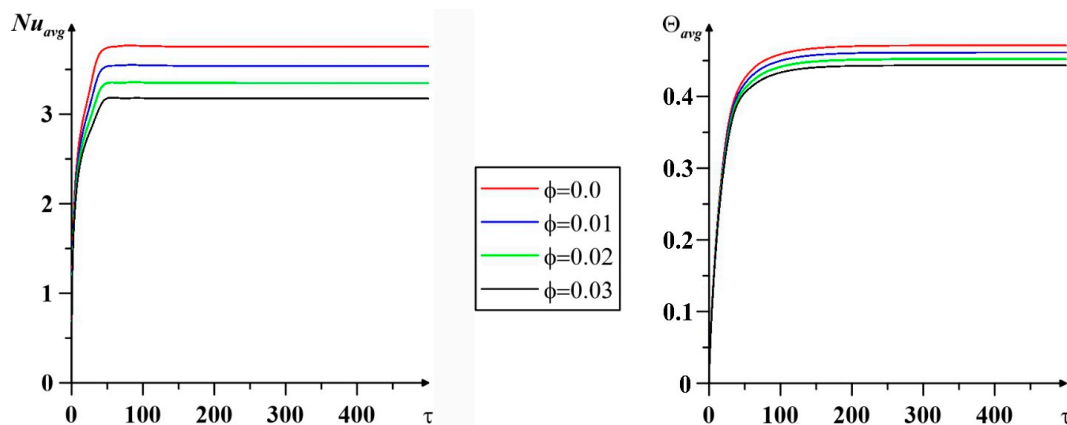


Figure 5. Nanoparticles' volume fraction influence on the average Nusselt number and mean temperature for one rib at $\delta = 0.2$.

An analysis of the nanoadditives' volume fraction influence was carried out for all options for the ribs number. It should be noted that the results in the cases of two and three ribs are similar; therefore, the ϕ effect is presented on the results of modeling the free convection in an enclosure with two solid ribs at $\delta = 0.2$.

It can be seen in Figure 6 that the flow structures were not changed significantly when the second rib was added; the cavity also contains two convective cells. Their size was reduced as the space for the fluid flow was reduced also with the addition of the second fin. In this case, it is noticeable that the streamline density changes with an increase in ϕ . In addition, according to the values of streamlines, it can be noted that the strength of the flow decreases with a growth in the nanoadditives' concentration. If we look closely at the isotherms, we can see that in the cases of $\phi = 0.0$ and 0.01 they practically coincide. Furthermore, the thermal plume degrades to an almost horizontal arrangement of isotherms. This means that in the latter case, the conductive mechanism of heat transfer predominates. At the same time, according to the nearest isotherm to the source, it can be seen that the temperature in the cavity noticeably increases with an increase in ϕ .

Figure 7 reflects the nanoparticles' concentration effect on the integral characteristics of the process at $\delta = 0.2$. Again, we note that with three fins, similar results are obtained; therefore, a variant with two fins is presented. It can be seen from the figure that the mean Nusselt number decreases with increasing ϕ , which illustrates the attenuation of convective energy transport. It should be noted that in the cases of $\phi = 0.0, 0.01, \text{ and } 0.02$, Nu_{avg} uniformly decreases by 0.1, but at $\phi = 0.03$, the decrease occurs only by 0.03. In this case, the average source temperature behaves differently. It can be seen that the cases of $\phi = 0.0$ and 0.01 coincided over time and have exactly the same values for the dimensionless time τ from 250 to the end. With further addition of nanoparticles, Θ_{avg} actively increases. In the case of $\phi = 0.03$, it has a maximum value, and also requires more time to reach the stationary regime.

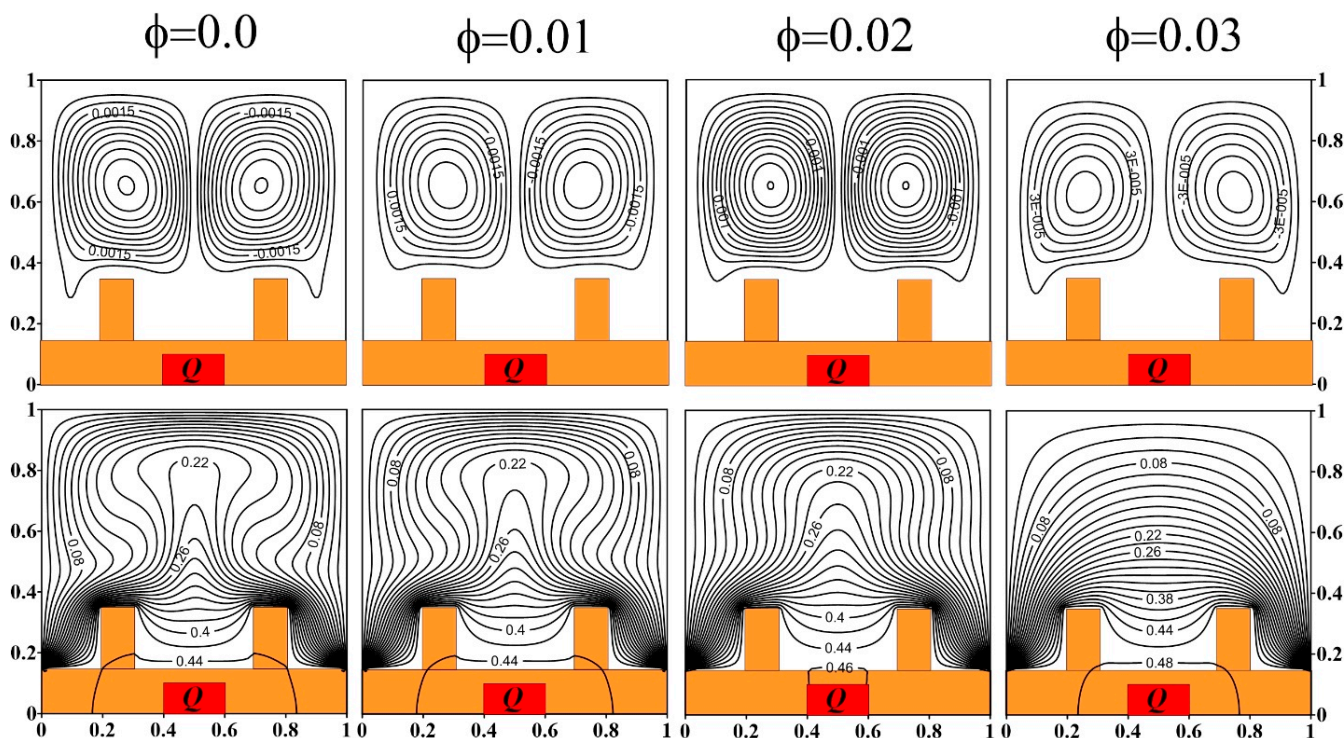


Figure 6. Nanoparticles' concentration influence on the streamlines and isotherms in the case of two fins at $\delta = 0.2$.

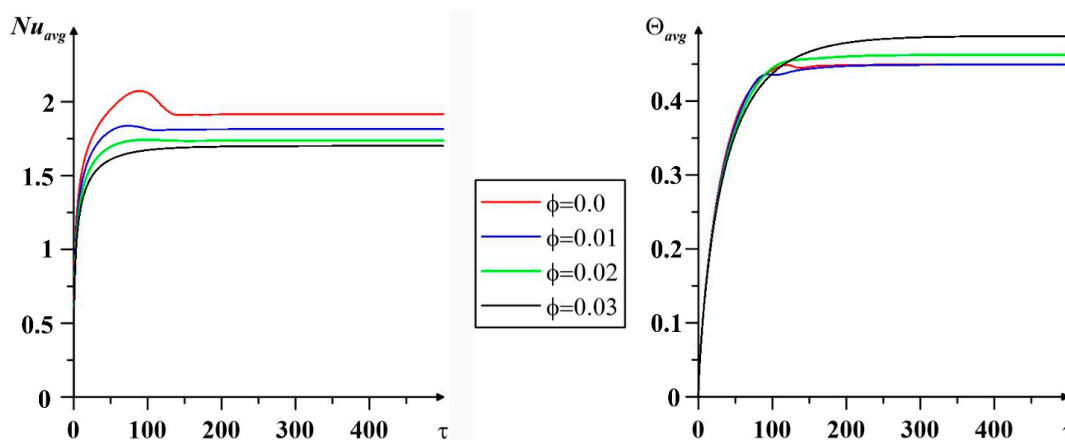


Figure 7. Nanoparticles' volume fraction influence on the average Nusselt number and mean temperature for two fins at $\delta = 0.2$.

Next, an analysis of the rib structure height influence was carried out. Figure 8 shows the distribution of streamlines and isotherms at $\phi = 0.01$ in the case of one rib. The isotherms show that two convective cells are preserved. Changes occurred only in the places where the cells adjoin the edge. Isotherms illustrate a two-dimensional heat plume. A rise in the fin height leads to compaction of the temperature isolines.

Figure 9 reflects the influence of changing the fin height on the mean Nusselt number and the average temperature in the heat-generated element at $\phi = 0.01$. It can be seen that both parameters decrease with an increase in δ . At the same time, Nu_{avg} decreases more actively than Θ_{avg} . It should be noted that at $\delta = 0.1$ and 0.2 , the temperature values practically coincide. The case $\delta = 0.3$ corresponds to the lowest temperature of the source, since in this case the enlarged fin removes heat more actively by means of a conductive heat exchange.

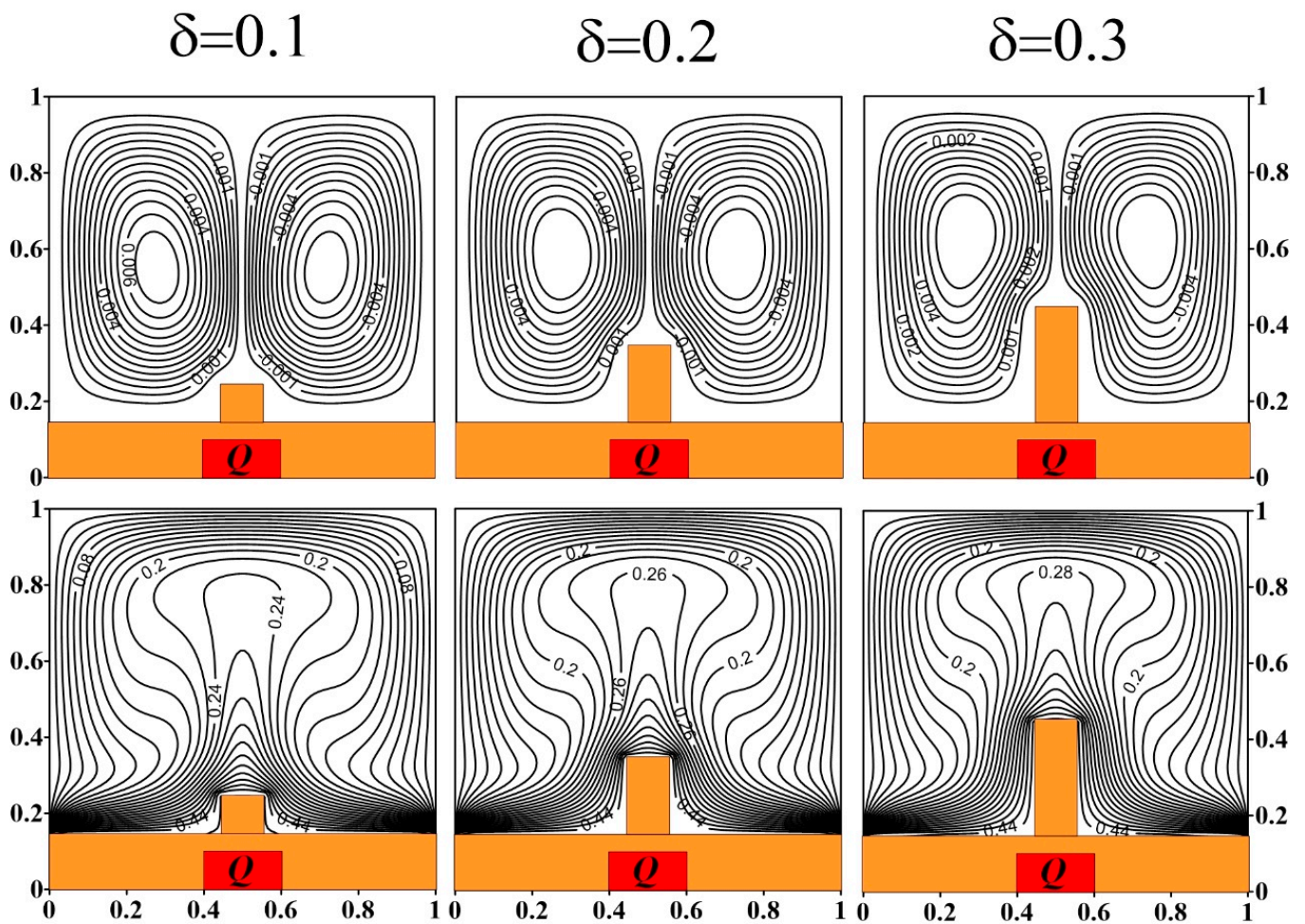


Figure 8. Effect of fin height on streamlines and isotherms at $\phi = 0.01$.

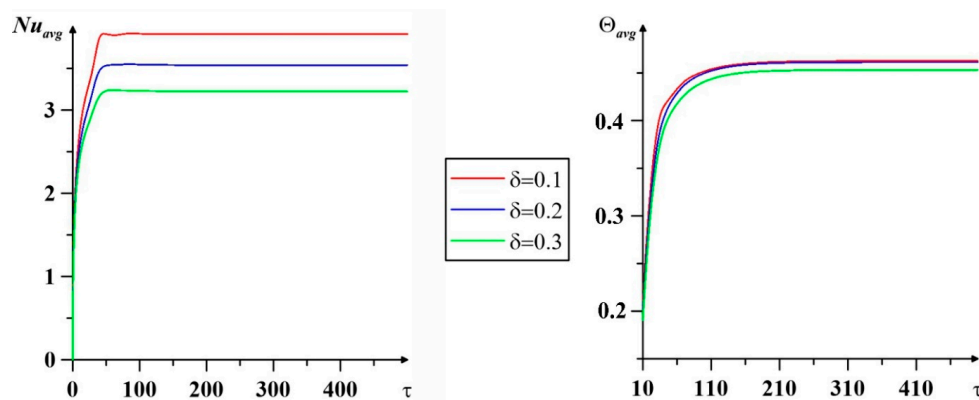


Figure 9. Effect of fin height on the mean Nusselt number and mean temperature at $\phi = 0.01$.

Next, we considered the influence of three ribs height in the cavity at $\phi = 0.01$. It should be noted that the results for two and three ribs are similar, so only three ribs are shown in Figure 10. The streamlines illustrate two convective cells in the chamber. The circulation for the right one is clockwise, while for the left one it is counterclockwise. With a rise in the fins' height, the size of the cells decreases, as well as the density of the streamlines. This is due to the reduced space for the fluid to flow. Note that in the case of $\delta = 0.3$, the cells almost take the form of a square. Isotherms also represent a two-dimensional heat plume. According to the isotherm closest to the source, we can trace the decrease in temperature: for $\delta = 0.1$ it is 0.46, for $\delta = 0.2$ it is 0.42, while for $\delta = 0.3$ it is 0.38. This result indicates an efficient cooling of the heated unit for three fins with a maximum height.

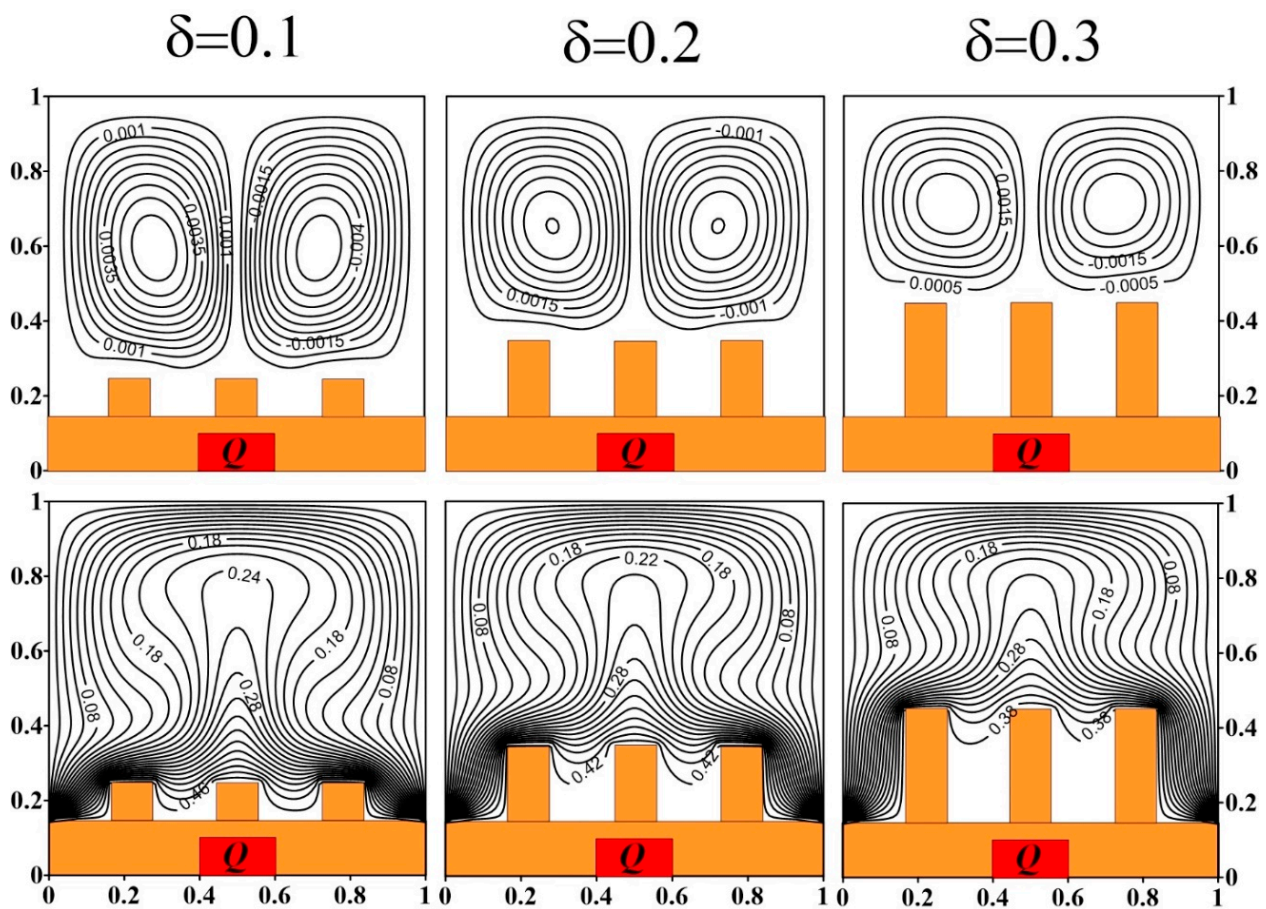


Figure 10. Effect of fin height on streamlines and isotherms in the case of three fins at $\phi = 0.01$.

Parameters Nu_{avg} and Θ_{avg} depending on the ribs' height and time are shown in Figure 11. Both parameters decrease with an increasing δ , as in the case of one rib. Despite the attenuation of convective energy transport in the chamber, the average source temperature also decreases. This phenomenon is also explained by the predominance of conductive energy transport.

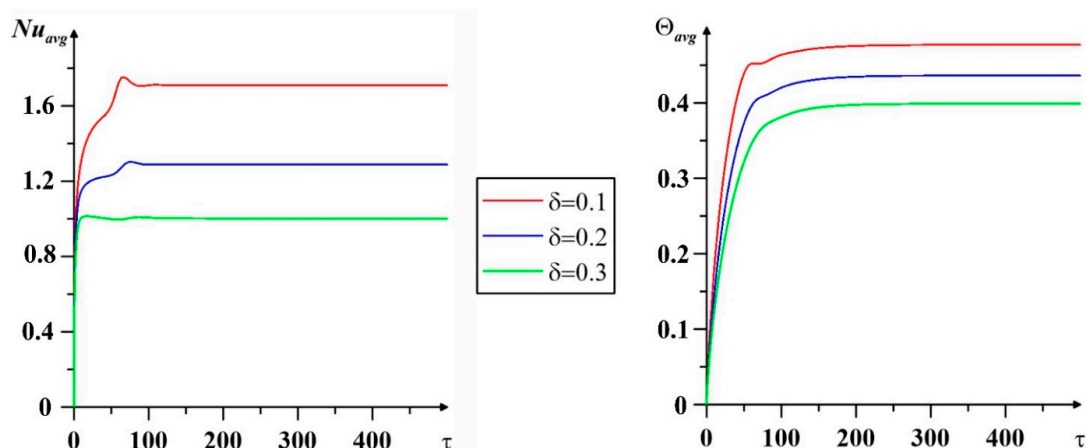


Figure 11. Impact of the fin height on the mean Nusselt number and mean temperature in the case of three fins at $\phi = 0.01$.

An assessment of the solid ribs number influence on the natural convective heat transfer is shown in Figure 12 at $\phi = 0.01$ and $\delta = 0.2$. It can be seen that the most intense convective heat transfer corresponds to calculations with one fin, because in this case Nu_{avg} has the maximum value. But for the same case, Θ_{avg} also has the maximum value. The most efficient cooling, taking into account

the selected parameters, occurs in the presence of three fins, despite the fact that the convective heat transfer is the weakest here.

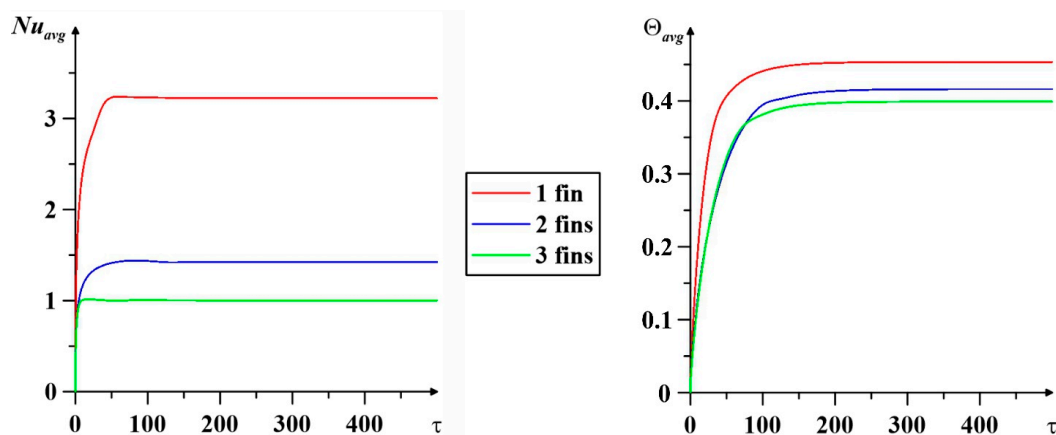


Figure 12. Impact of the fins number on the average Nusselt number and average temperature at $\phi = 0.01$, $\delta = 0.2$.

4. Conclusions

Mathematical modeling of the power-law nanoliquid natural convection in an enclosure with a solid heat sink and a heater of constant internal volumetric heat generation was carried out in this study. In the course of the work, the influence of the nanoadditives' concentration ($\phi = 0.0-0.03$), the ribs' height ($\delta = 0.1-0.3$) and their number on the intensification of the heated element cooling was analyzed. The analysis of the results allowed us to draw the following conclusions:

1. An increase in the concentration of nano-additives in the case of one rib leads to a decrease in the average temperature of the heater, while in the case of two ribs, an increase in the average temperature of the heater is observed with a reduction in the nanoparticles' concentration. Therefore, it is necessary to perform additional analysis for the nanoparticles' concentration influence that depends on the fins number.
2. Increasing the fin height makes it possible to intensify the cooling of the source with any solid fins number.
3. The lowest average source temperature corresponds to the presence of three fins in the cooling system.

The performed analysis showed advantages of the considered cooling system. In future, this formulation can be extended to the following cases—porous finned heat sink, a heat-generating element of variable internal volumetric heat flux, three-dimensional analysis.

Author Contributions: Conceptualization, M.A.S.; methodology, M.A.S.; software, D.S.L.; validation, D.S.L.; investigation, D.S.L.; writing—original draft preparation, D.S.L. and M.A.S.; writing—review and editing, D.S.L. and M.A.S.; visualization, D.S.L.; supervision, M.A.S. All authors have read and agreed to the published version of the manuscript.

Funding: This work was conducted as a government task of the Ministry of Science and Higher Education of the Russian Federation (Project Number FSWM-2020-0036).

Data Availability Statement: Not applicable.

Conflicts of Interest: The authors declare no conflict of interest.

References

1. Ganesh, N.V.; Al-Mdallal, Q.M.; Hirankumar, G.; Kalaivanan, R.; Chamkha, A.J. Buoyancy-driven convection of MWCNT—Casson nanofluid in a wavy enclosure with a circular barrier and parallel hot/cold fins. *Alex. Eng. J.* **2022**, *61*, 3249–3264. [[CrossRef](#)]
2. Nemati, H. A general equation based on entropy generation minimization to optimize plate fin heat sink. *Eng. J.* **2018**, *22*, 159–174. [[CrossRef](#)]
3. Prabowo, A.D.; Amrizal; Ibrahim, G.A. Geometry optimization of PV/T-TEG collector under different operating conditions using CFD simulation and Taguchi method. *Eng. J.* **2022**, *26*, 1–11. [[CrossRef](#)]

4. Hatami, M. Numerical study of nanofluids natural convection in a rectangular cavity including heated fins. *J. Mol. Liq.* **2017**, *233*, 1–8. [[CrossRef](#)]
5. Hidki, R.; El Moutaouakil, L.; Boukendil, M.; Charqui, Z.; Zrikem, Z.; Abdelbaki, A. Impact of Cu/Al₂O₃-water hybrid nanofluid on natural convection inside a square cavity with two heat-generating bodies. *Mater. Today Proc.* **2023**, *72*, 3749–3756. [[CrossRef](#)]
6. Iftikhar, B.; Javed, T.; Siddiqui, M.A. Natural convective flow of non-isothermal hybrid nanofluid inside the cavity with the influence of a heated fin and non-linear thermal radiation: Second law analysis. *Mater. Today Commun.* **2023**, *34*, 105341. [[CrossRef](#)]
7. Waqas, H.; Khan, S.A.; Yasmin, S.; Liu, D.; Imran, M.; Muhammad, T.; Alhushaybari, A.; Farooq, U. Galerkin finite element analysis for buoyancy driven copper-water nanofluid flow and heat transfer through fins enclosed inside a horizontal annulus: Applications to thermal engineering. *Case Stud. Therm. Eng.* **2022**, *40*, 102540. [[CrossRef](#)]
8. Shahsavar, A.; Rashidi, M.; Yıldız, Ç.; Arıcı, M. Natural convection and entropy generation of Ag-water nanofluid in a finned horizontal annulus: A particular focus on the impact of fin numbers. *Int. Commun. Heat Mass Transf.* **2021**, *125*, 105349. [[CrossRef](#)]
9. Tayebi, T.; Dogonchi, A.S.; Karimi, N.; Ge-JiLe, H.; Chamkha, A.J.; Elmasry, Y. Thermo-economic and entropy generation analyses of magnetic natural convective flow in a nanofluid-filled annular enclosure fitted with fins. *Sustain. Energy Technol. Assess.* **2021**, *46*, 101274. [[CrossRef](#)]
10. Yasmin, S.; Khan, S.A.; Fatima, N.; Imran, M.; Tahir, M.; Waqas, H.; Farooq, U.; Xu, Y.-J. Computational analysis of MHD MgO—Water nanofluid flow inside hexagonal enclosure fitted with fins. *Case Stud. Therm. Eng.* **2023**, *43*, 102788. [[CrossRef](#)]
11. Hejri, S.; Malekshah, E.H. Cooling of an electronic processor based on numerical analysis on natural convection and entropy production over a dissipating fin equipped with copper oxide/water nanofluid with Koo-Kleinstreuer-Li model. *Therm. Sci. Eng. Prog.* **2021**, *23*, 100916. [[CrossRef](#)]
12. Al-Farhany, K.; Al-Chlahawi, K.K.; Al-dawody, M.F.; Biswas, N.; Chamkha, A.J. Effects of fins on magnetohydrodynamic conjugate natural convection in a nanofluid-saturated porous inclined enclosure. *Int. Commun. Heat Mass Transf.* **2021**, *126*, 105413. [[CrossRef](#)]
13. Yan, S.-R.; Pordanjani, A.H.; Aghakhani, S.; Goldanlou, A.S.; Afrand, M. Management of natural convection of nanofluids inside a square enclosure by different nano powder shapes in presence of fins with different shapes and magnetic field effect. *Adv. Powder Technol.* **2020**, *31*, 2759–2777. [[CrossRef](#)]
14. Siavashi, M.; Yousofvand, R.; Rezanejad, S. Nanofluid and porous fins effect on natural convection and entropy generation of flow inside a cavity. *Adv. Powder Technol.* **2018**, *29*, 142–156. [[CrossRef](#)]
15. Esfe, M.H.; Barzegarian, R.; Bahiraei, M. A 3D numerical study on natural convection flow of nanofluid inside a cubical cavity equipped with porous fins using two-phase mixture model. *Adv. Powder Technol.* **2020**, *31*, 2480–2492. [[CrossRef](#)]
16. Gireesha, B.J.; Sowmya, G.; Khan, M.I.; Öztop, H.F. Flow of hybrid nanofluid across a permeable longitudinal moving fin along with thermal radiation and natural convection. *Comput. Methods Programs Biomed.* **2020**, *185*, 10516. [[CrossRef](#)]
17. Aly, A.M.; Mohamed, E.M.; Alsedais, N. Double-diffusive convection from a rotating rectangle in a finned cavity filled by a nanofluid and affected by a magnetic field. *Int. Commun. Heat Mass Transf.* **2021**, *126*, 105363. [[CrossRef](#)]
18. Siva, T.; Jangili, S.; Kumbhakar, B.; Mondal, P.K. Unsteady electromagnetohydrodynamic flow of couple stress fluid through a microchannel: A theoretical analysis. *Eur. J. Mech.-B/Fluids* **2022**, *95*, 83–93. [[CrossRef](#)]
19. Mehta, S.K.; Mondal, P.K. Free convective heat transfer and entropy generation characteristics of the nanofluid flow inside a wavy solar power plant. *Microsyst. Technol.* **2023**, *29*, 489–500. [[CrossRef](#)]
20. Mondal, P.K.; Wongwises, S. Magneto-hydrodynamic (MHD) micropump of nanofluids in a rotating microchannel under electrical double-layer effect. *J. Process Mech. Eng.* **2020**, *234*, 318–330. [[CrossRef](#)]
21. Nabwey, H.A.; Rashad, A.M.; Khan, W.A.; Alshber, S.I. Effectiveness of magnetize flow on nanofluid via unsteady natural convection inside an inclined U-shaped cavity with discrete heating. *Alex. Eng. J.* **2022**, *61*, 8653–8666. [[CrossRef](#)]
22. Khan, A.U.; Ullah, N.; Al-Zubaidi, A.; Nadeem, S. Finite element analysis for CuO/water nanofluid in a partially adiabatic enclosure: Inclined Lorentz forces and porous medium resistance. *Alex. Eng. J.* **2022**, *61*, 6477–6488. [[CrossRef](#)]
23. Khezzar, L.; Siginer, D.; Vinogradov, I. Natural convection of power law fluids in inclined cavities. *Int. J. Therm. Sci.* **2012**, *53*, 8–17. [[CrossRef](#)]
24. Guo, S.S.; Luo, Z.Y.; Tao, W.; Zhao, J.F.; Cen, K.F. Viscosity of monodisperse silica nanofluids. *Bull. Chin. Ceram. Soc.* **2006**, *25*, 52–55.
25. Jang, S.P.; Choi, S.U.S. Effects of various parameters on nanofluid thermal conductivity. *J. Heat Transf.* **2007**, *129*, 617–623. [[CrossRef](#)]
26. Loenko, D.S.; Sheremet, M.A. Regularization models for natural convection of a pseudoplastic liquid in a closed differentially heated cavity. *Bull. Perm Univ. Phys.* **2021**, *3*, 13–22. [[CrossRef](#)]
27. Loenko, D.; Shenoy, A.; Sheremet, M. Influence of the chamber inclination angle and heat-generating element location on thermal convection of power-law medium in a chamber. *Int. J. Numer. Methods Heat Fluid Flow* **2021**, *31*, 134–153. [[CrossRef](#)]
28. Shenoy, A.; Sheremet, M.; Pop, I. *Convective Flow and Heat Transfer from Wavy Surfaces: Viscous Fluids, Porous Media and Nanofluids*; CRC Press: Boca Raton, FL, USA, 2016; p. 306.
29. Turan, O.; Sachdeva, A.; Chakraborty, N.; Poole, R.J. Laminar natural convection of power-law fluids in a square enclosure with differentially heated side walls subjected to constant temperatures. *J. Non-Newton. Fluid Mech.* **2011**, *166*, 1049–1063. [[CrossRef](#)]

Disclaimer/Publisher’s Note: The statements, opinions and data contained in all publications are solely those of the individual author(s) and contributor(s) and not of MDPI and/or the editor(s). MDPI and/or the editor(s) disclaim responsibility for any injury to people or property resulting from any ideas, methods, instructions or products referred to in the content.